Groundwater controls on colloidal transport in forest stream waters

N. Gottselig[a], J. Sohrt[b], D. Uhlig[c,d], V. Nischwitz[e], M. Weiler[b], W. Amelung[a,d]*

[a]Institute of Crop Science and Resource Conservation, Soil Science and Soil Ecology, University of Bonn, Nussallee 13, 53115 Bonn, Germany

[b]Chair of Hydrology, Albert-Ludwigs-Universität Freiburg, Friedrichstraße 39, 79098 Freiburg, Germany

[c]GFZ German Research Centre for Geosciences, Section Earth Surface Geochemistry, Telegrafenberg, 14473 Potsdam, Germany

[d]Forschungszentrum Jülich GmbH, Institute of Bio- and Geosciences, IBG-3: Agrosphere, 52425 Jülich, Germany

[e]Forschungszentrum Jülich GmbH, Central Institute for Engineering, Electronics and Analytics (ZEA-3), 52425 Jülich, Germany

*: Corresponding author; email: ngottsel@uni-bonn.de

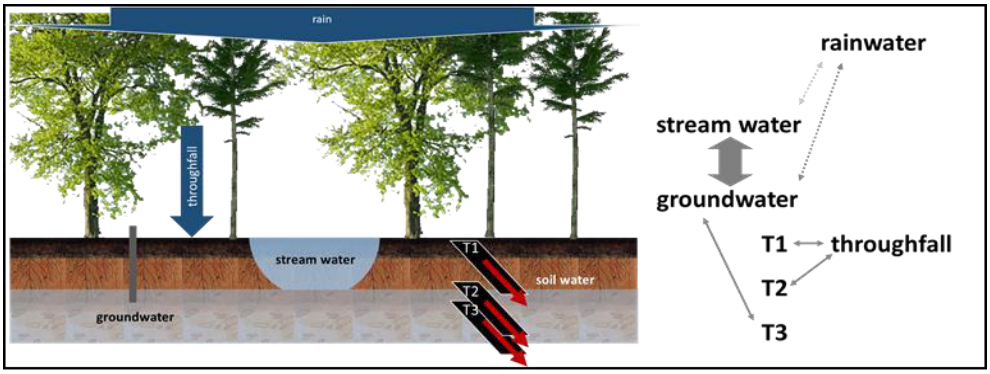
rain
throughfall
stream water
soil water
groundwater
T1
T2
T3
rainwater
stream water
groundwater
T1
throughfall
T2
T3

Highlights:

- The origin of colloids in streams indicates elemental transport pathways.
- Monthly analysis of stream & groundwater, rainwater, throughfall, soil leachate.
- Field flow fractionation revealed three fractions in all sample types.
- Groundwater derived colloids dominated the stream signal.
- Water flux and particle reformation affect the seasonal dynamics of particles.

Abstract

Biogeochemical changes of whole catchments may, at least in part, be deduced from changes in stream water composition. We hypothesized that there are seasonal variations of natural nanoparticles (NNP; 1-100 nm) and fine colloids (<300 nm) in stream water, which differ in origin depending on catchment inflow parameters. To test this hypothesis, we assessed the annual dynamics of the elemental composition of NNP and fine colloids in multiple water compartments, namely in stream water, above and below canopy precipitation, groundwater and lateral subsurface flow from the Conventwald catchment, Germany. In doing so, we monitored meteorological and hydrological parameters, total element loads, and analyzed element concentrations of org C, Al, Si, P, Ca, Mn and Fe by Asymmetric Flow Field Flow Fractionation (AF^4). The results showed that colloid element concentrations were <5 µmol/L. Surprisingly, up to an average of 55 % (Fe) of total element concentrations were not truly dissolved but bound to NNP and fine colloids. The colloid patterns showed seasonal variability with highest loads in winter. The presence of groundwater-derived colloidal Ca in stream water showed that groundwater mainly fed the streams throughout the whole year. Overall, the results showed that different water compartments vary in the NNP and fine colloidal composition making them a suitable tool to identify the streams NNP and fine colloid sources. Given the completeness of the dataset with respect to NNP and fine colloids in multiple water compartments of a single forest watershed this study adds to the hitherto underexplored role of NNP and fine colloids in natural forest watersheds.

1. Introduction

Forest ecosystems critically link the earth's water and nutrient cycles, making them vital components of the global ecosystem (Perry et al., 2008). Therefore, studying pristine forests may provide a benchmark for the natural cycling of elements in terrestrial environments. The element loss from such an ecosystem is largely reflected by the element load in stream waters. Frequently, samples are filtered to gain an operationally defined dissolved phase (<0.45 µm) of elements. This definition, however, takes the risk of including very fine particles in the size range of natural colloids (1 nm-1 µm), specifically of nanoparticles (NNP, 1-100 nm), the presence of which may alter the bioavailability of the elements and thus subsequent interpretations from studying stream water composition. The consideration of colloids and especially NNP is highly relevant as up to 90-100% of the elements Fe, P, Mn, Al and organic carbon (org C), for instance, have been detected in the specific size range of NNP and colloids and not in dissolved state (Baalousha et al., 2011; Baken et al., 2016b; Gottselig et al., 2017a; Jarvie et al., 2012; Missong et al., 2018a). To understand the processes governing the biogeochemical cycling of elements in forested watersheds, a prerequisite is to link NNP and colloid mediated transport/export with hydrological processes determining the flow of the particle transport medium water.

As a subset of colloids, NNP are of particular interest as elemental carrier due to their higher specific surface area in comparison to larger sized colloids or particles (Hartland et al., 2013). The reactivity of NNP renders them potentially predominant carriers of limiting nutrients such as P in headwater catchments. Fundamental building blocks of NNP in acidic freshwaters and carriers of multiple further elements are most frequently Fe and/or org C (Andersson et al., 2006; Neubauer et al., 2013), and clay minerals in the fine colloidal size range (100-450 nm) (Gottselig et al., 2017b; Hill and Aplin, 2001; Missong et al., 2018b). In so far as the chemical

composition of these particles is preserved during transport within the catchment, it can be used as an indicator of the potential origin of the stream's NNP and colloids. For this purpose, NNP and colloids must be analyzed from the entirety of water compartments contributing to the stream, i.e., in rainwater and throughfall, as well as in lateral subsurface flow, ground- and stream water.

To our knowledge there is only one single study of NNP and colloids in rainwater and throughfall from Gandois et al. (2010). They assigned an important role to local atmospheric emissions for the composition of rainwater particles, whereas dry deposition and canopy leaching modified the chemical composition of particles carried by throughfall. Gandois et al. (2010) additionally reported that complexation with organic matter promoted formation and dissolution of colloids in throughfall; specifically Al, Fe and Pb were found associated to org C. Yet, Gandois et al. (2010) restricted their analysis to bulk deposition and throughfall samples collected weekly over one year and, therefore, could not compare their data to soil, stream or groundwater of the same catchment.

In contrast to precipitation waters, NNP and colloids dispersed or leached from soil are usually substantially higher concentrated and likely exhibit a more diverse elemental composition. Missong et al. (2018b) attempted a first comparison between colloids from soil leachates (Missong et al., 2018b), soil extracts (Missong et al., 2018a) and stream water colloids (Gottselig et al., 2017b) of the same sites and found a close similarity between stream water and soil leachate NNP and colloids. A common feature of all three sample types was the detection of an org C-rich NNP fraction <20-25 nm, which also contains Fe, Al, Mn, Ca and P; as also reported by other studies (Baken et al., 2016b; Gottselig et al., 2014; Gottselig et al., 2017b; Haygarth et al., 1997; Jiang et al., 2015; Regelink et al., 2013; Regelink et al., 2014). The chemical composition of NNP between 20/25 nm to 60/70 nm matches between stream

waters and soil leachates, showing dominant concentrations of org C, Fe, Al and P (Gottselig et al., 2017b; Missong et al., 2018b), but these fractions can also contain substantial amounts of Ca and Mn (Gottselig et al., 2017a). Extracted soil particles 25-240 nm were dominated by Fe (Missong et al., 2018a) and potentially include instable, artificially mobilized particles (Missong et al., 2018b) that are either filtered or decay and thus likely do not reach the streams or groundwater bodies. Particles extracted from soil usually exhibited a wider size range of particles (up to 500 nm) than streams or leachates (up to 300-400 nm). It is therefore necessary to elucidate the presence of colloid fractions in all water compartments within a forested watershed to deduce conclusions on intercompartment mobility.

Nanoparticle transport at saturated flow may reach the groundwater if colloid phase stability is given (Degueldre et al., 2000) and when the topsoil is hydraulically connected to groundwater at moist conditions. Studies on the elemental presence in groundwater agree that the composition of the bedrock surrounding the aquifer dominates the general elemental composition found in the groundwater (e.g. Rosenthal, 1987). The same is also valid for potentially present colloids (Degueldre et al., 2000). Surprisingly, data on groundwater colloids is scarce (Baalousha et al., 2011). The studies of Cizdziel et al. (2008) and Baik et al. (2007) have identified NNP in groundwater but also larger sized colloids containing a variety of elements. Saito et al. (2015) compared the chemical composition of colloids in groundwater draining sedimentary and granitic bedrock and also found some larger inorganic colloids. Despite low concentrations, NNP fractions <10 nm dominated mass fluxes for both groundwater aquifers. The exact origin of the NNP remained open.

Through temporal imbalances of recharge and drainage, most groundwater bodies display a seasonally fluctuating water table. Previous analyses of stream waters has revealed that Fe, Al, org C and limiting nutrients, such as P, were predominantly present in NNP and colloidal

fractions (Fernández-Martínez et al., 2014; Gottselig et al., 2017a; Hart et al., 1993; Hill and Aplin, 2001; Jarvie et al., 2012; Martin et al., 1995). The analysis of seasonal dynamics shed new light on the reasoning behind the occurrence of these elements in the colloidal fractions (Dahlqvist et al., 2004; Dahlqvist et al., 2007; Pokrovsky et al., 2010). During the spring flood, both the total load of transported colloids in stream water and the element concentrations adhered to colloids were elevated (Pokrovsky et al., 2010). Also, seasonal changes in the flow regime modify transport pathways of NNP and colloids and thereby affect the chemical composition of NNP and colloids. In winter, for example, Fe serves as building block of NNP and colloids in stream waters due to inflow of anoxic groundwater, whereas precipitation and/or snow melt in early spring largely leach organic-rich top soil layers during flood and following hydrological events, thus potentially shifting the colloidal composition to a dominance of org C (Dahlqvist et al., 2004; Dahlqvist et al., 2007). In contrast, hydrological pathways in late spring/early summer frequently focus on groundwater recharge than on stream water inflow with exception of the afore mentioned rain events (Dahlqvist et al., 2007). It seems therefore reasonable to assume that there will also be a pronounced seasonal variability of NNP and colloidal bound elements.

Seasonal variability of dissolved and colloid-bound elements might be closely linked to discharge, so that their log-log transformed concentration-discharge (C-Q) ratio can facilitate the distinction between elements governed by dilution (C-Q slope ≤ -0.1), chemostatic ($-0.1 <$ slope < 0.1) or enrichment (slope ≥ 0.1) process controls (Trostle et al., 2016). This relationship can moreover yield relevant information about the origin of discharge waters, how they vary and thus govern particle mediated export in different catchments (e.g. Perdrial et al., 2014; Trostle et al., 2016). An observed enrichment of NNP and colloids and elements occurs simultaneously in conditions favoring particle adherence, particularly when organic matter is

present to stabilize particles (Herndon et al., 2015; Ranville and Macalady, 1997; Six et al., 1999), whereas, in turn, dilutive conditions can indicate discharge waters originating from inflows with lacking presence of typical NNP and colloid building blocks but with high Ca and/or Si concentrations (Haygarth et al., 2004; Herndon et al., 2015; Maher, 2011).

In summary we note that a detailed understanding of seasonal variations of colloids vs. truly dissolved (<1 nm) elements in terrestrial water catchments is still lacking. In addition, the knowledge on the potential origin of the particles is limited. We hypothesize that there are seasonal variations of NNP and larger colloids during the year in stream water, which differ in origin depending on connectivity to the groundwater. Yet, and even though runoff generation in a catchment is composed of groundwater, precipitation and stream water, the holistic analysis of their NNP and colloid mass fluxes is rarely done, especially not over the course of one year. To highlight the respective interactions, we monitored NNP and fine colloid fractions as well as their corresponding elemental concentrations in monthly samples from several components of the hydrological cycle, i.e., of rainwater, throughfall, subsurface flow, stream and groundwater in accordance to hydrological monitoring of stream water discharge, groundwater level and precipitation amounts. The assessment of NNP and fine colloids was performed after Field Flow Fractionation (FFF), a non-destructive chromatography-like technique, which can be coupled to mass spectrometry and other element-specific detectors, and is routinely applied to distinguish NNP and colloids in environmental samples (Baalousha et al., 2011; Nischwitz et al., 2018).

2. Material and methods

2.1 Study site

Samples were obtained from the Conventwald study site, which is situated in the Black Forest (48°02'0 N, 7°96'0 E) near Freiburg, Germany. The site is a Level II intensive monitoring site of the Pan-European International Co-operative Program on assessment and monitoring of air pollution effects on forests (ICP Forests) under UN-ECE (Lang et al., 2017; Lorenz, 1995; Vries et al., 2003). Two small neighboring catchments were sampled, catchment 1 with an area of 0.086 km² and to the east catchment 2 with an area of 0.077 km² (Sohrt, 2019). Both have an average elevation of 840 m a.s.l., an average slope angle of 20°, annual mean temperatures around 6.6°C, and a mean annual precipitation of 1749 mm a^{-1} (see also Lang et al. (2017) for more details). The soils are Cambisols (IUSS, 2015), developed from paragneiss. Dominant tree species are *Fagus sylvatica, Picea abies* and *Abies alba*. Catchment 1 is drained by a creek and catchment 2 by a spring without visible surface flow.

Scientific instrumentation of catchment 1 was done some decades ago by the 'Forstliche Versuchs- und Forschungsanstalt Baden-Württemberg', Freiburg, Germany, and consists of above- and below-canopy precipitation collectors, soil moisture sensors and a discharge weir at the catchment outlet. Catchment 2 was instrumented in 2013/2014 by the University of Freiburg, with above- and below-canopy rainwater collectors, a weir at the catchment outlet, and lateral subsurface flow samplers (10 m wide refilled trench) and with a groundwater well by GFZ Potsdam.

2.2 Sampling

Monthly samples were collected from February 2015 to February 2016 from the above- and below-canopy precipitation collectors (termed rainwater and throughfall), the groundwater

well, stream and spring weirs of catchments 1 and 2 as well as at the first surface visible stream flow of catchment 1 ("spring"; supplementary information, Table SI1). Additionally, samples integrating lateral subsurface flow from three trench depth intervals were collected (collection at 10 cm depth: integration of depth 0-10 cm, 230 cm depth: 10-230 cm and 300 cm depth: 230-300 cm; supplementary information, Table SI1, for further details). Not all samples were available at all sampling dates (supplementary information, Table SI1). Samples were taken in 250 mL PE bottles. Prior to analyses, samples were stored at 4°C and analyzed within two weeks. An overview of sampling dates and discharge is provided in Figure SI1 (supplementary information).

2.3 Hydrological and meteorological parameters

During the sampling period, meteorological data (air temperature, precipitation amounts above and below the tree canopy) were recorded every 15 min and hydrological data (current discharge at the weirs, soil moisture in 30 and 60 cm depth, the height of the groundwater level) every 5 min (Figure 1; supplementary information, Figure SI2). The groundwater level was determined via a pressure probe installed in 8.5 m below the surface. Above and below tree canopy precipitation was collected via self-constructed rain collectors and amounts were determined through direct scale reading.

In addition to the parameters recorded in the field, pH and electrical conductivity (EC) of the stream water samples at catchment 2 weir as well as EC of the groundwater samples was recorded in the laboratory immediately after sampling (supplementary information, Figure SI2). To determine the relative contributions of groundwater vs. lateral subsurface flow into the stream, concentrations of eight elements (Ca, Na, K, Mg, S, DOC, Si, Cl) were analyzed in stream water, groundwater and the three depths of lateral subsurface flow collection and

used for end-member-mixing-analysis (EMMA; calculated according to Dietze and Dietze, 2013, see also Sohrt 2019). The elements were selected on the basis of recent literature (e.g. Barthold et al., 2011; Frisbee et al., 2011; Guinn Garrett et al., 2012). The results and robustness of the EMMA are shown in the supplementary information, Figure SI2.

2.4 Particle fractionation and concentration data

Samples were not filtered prior to analyses, in order to prevent clogging of the filter. Thus, particle fractionation was directly performed via Asymmetric Flow Field Flow Fractionation (AF^4, Postnova Analytics, Landsberg, Germany) coupled to a UV detector, a quadrupole inductively coupled plasma-mass spectrometer with helium collision cell technology (ICP-MS; Agilent 7500, Agilent Technologies, Japan) and an organic carbon detector (OCD; DOC Labor, Karlsruhe, Germany). This method is particularly suitable for aqueous samples because they can be analyzed in their natural state without undergoing prior processing. Fractionation parameters, ICP-MS system settings and calibration as well as OCD coupling parameters and calibration can be found in section 2.2 of Gottselig et al. (2017a). Total concentrations of org C were assessed for the first six months of the sampling period (Feb 2015 to Jul 2015) and of Al, Si, P, Ca, Mn and Fe for the second half of the sampling period (Aug 2015 to Feb 2016). Colloidal org C concentrations were often below detection limit (LOD = 0.001 mmol L^{-1}).

NNP and fine colloids from aqueous samples were also compared to water dispersible colloids (WDC), which were extracted from soil horizon aliquots of a soil pit sampling performed in Nov 2013. The WDC extraction was performed and published by Missong et al. (2018a). Total element concentrations of the soil horizons as well as further information on the soil pit study can be found in Lang et al. (2017). WDC and total soil data were transferred to the unit µmol g_{soil}^{-1} for better comparison.

2.5 Data analysis

The ICP-MS raw data were collected in counts per second (cps) by the MassHunter Workstation Software (Agilent Technologies, Japan), and OCD raw data were recorded in volt detector signal (V) with the AF^4 analytical software (Postnova Analytics, Landsberg, Germany). Both datasets were exported to Excel (Microsoft Corporation, Redmond, USA) for baseline correction, peak integration and calculation of peak concentrations through multipoint linear calibrations. In general, the particle data is referred to as $1^{st}/2^{nd}/3^{rd}$ fraction of element X and all colloidal element concentration refers to the sum of the elements concentrations in the 1^{st}, 2^{nd} and 3^{rd} fraction. All concentration data were transferred to µmol L^{-1} for Al, Si, P, Ca, Mn and Fe and to mmol L^{-1} for org C. Additionally, total elemental concentrations in the samples were determined via the ICP-MS and the OCD, respectively. In contrast to the ICP-MS, which also functions as a stand-alone device, the OCD measurements for total org C were realized by direct injection through the AF^4 autosampler.

The relative proportion of particles was determined by calculating the percentage of all colloidal elemental concentration of each element with respect to the total elemental concentration of each element in the respective sample. The truly dissolved (<1 kDa) elemental concentrations are derived as difference between the total and all colloidal concentration per element.

For comparability reasons the concentration data measured in samples from the weirs of catchment 1 and 2 over the 13 month sampling period were multiplied by discharge amount at time of sampling and thus expressed as loads in the unit (µ/m)mol s^{-1}. Additionally, to analyze the variability of elemental concentrations in the fractions over the sampling duration, the sum of all colloidal element contents was set to 100% and the fraction concentrations

were then expressed in percentages of the total colloidal fraction. Predictions of colloidal concentrations and stream water inflows were performed after all input data underwent $\log_{10}$ transformations. Pearson correlations ($p<0.05$) were calculated using Statistica 8.0 (StatSoft Europe, Hamburg, Germany).

2.6 Process and quality control

The storage capability and thus transportability of natural nanoparticles and colloids after sampling is decisively determined by the stability of the particle composition and sizes as collected when sampling. A first detailed assessment of the circumstances affecting colloidal stability was conducted by Buffle and Leppard (1995). They recommended to keep storage times as short as possible. Own unpublished work has revealed that constant refrigerated storage of unprocessed stream water in pre-cleaned polyethylene or polypropylene containers sustained a stability of natural colloids at least up to 14 days after sampling. Prior to taking the actual sample, containers were preconditioned in triplicates with stream water and the sample was taken from the center of the flowing stream without disturbance of sediments. Visible fractions of leaves or further debris was not included in the sample, nor was the sample processed in any way except agitation prior to injection into the AF^4.

The AF^4 is in theory capable of resolving the whole size spectrum between 1 and 1000 nm within one fractionation run, yet the application, especially to environmental particles, has proven that an optimal resolution can only be achieved when focusing on a size range with a width of about 500 nm. Due to the aspired redefinition of the operationally defined dissolved phase (<0.45 µm), we focused on particles between 1 and 450/500 nm. Extensive method development was conducted for the AF^4 fractionation of stream water to target this particle size range (Gottselig et al., 2014; Gottselig et al., 2017b). Through variation of fractionation

parameters (mainly cross flow rate and gradient), it was possible to achieve a resolution of three particle fractions: 1-20 nm, >20-60 nm, >60-300 nm. Steric elution could be excluded because void peaks were often lacking or negligibly small. Thus, the majority of particles in the stream water samples measured to date are within the size range of 1 to 300 nm and included in the <0.45 µm fraction.

The AF^4 fractionation is achieved despite the absence of a stationary phase. Yet, interactions with the membrane defining the lower particle size cut-off cannot be neglected, especially during focusing of the sample and/or at high cross flows. As reference parameter, the total sample concentration per element prior to fractionation was always recorded offline by ICP-MS. The comparison of total and all particulate data yielded elemental concentrations in the colloidal fraction up to 99.5% of total elemental concentrations, thus allowing the conclusion that no major particle loss occurs (Gottselig et al., 2017a). A detailed investigation of the AF^4 recoveries of synthetic iron oxyhydroxide colloids revealed recoveries between 70 and 93% (Baken et al., 2016a). These results are transferrable to natural particles given the similarity of synthetic iron oxyhydroxides with natural particles.

3. Results

3.1 Particle fractionation

The fractionation of the aqueous samples with AF^4 coupled online to ICP-MS or OCD resulted in three distinct particle peaks, whereby the 2^{nd} fraction was dominated by Ca (Figure 2). Peak boundaries were defined by the changing ICP-MS signal intensities between the monitored elements. A similar peak pattern for aqueous samples in general was previously observed for several other stream water samples in Europe (Gottselig et al., 2017a; Gottselig et al., 2017b).

In Gottselig et al. (2017b), samples from the Conventwald catchment were also included and size measurements of the particle fractions reported. Also the particle sizes at the peak boundaries were similar to those previously observed for other forest ecosystems (Gottselig et al., 2017a; Gottselig et al., 2017b), reflecting a reproducible fractionation process for similar sample types (section 2.6). The smallest particle size of the 1st fraction was equal to the molecular weight cut-off (MWCO) of the membrane (1kDa; equivalent to r~0.66 nm, equation 2.2, Erickson 2009) and included particles up to approx. 20 nm hydrodynamic diameter, the 2nd fraction included nanoparticles between 20 and 60 nm and the 3rd fraction nanoparticles >60 nm to colloids of a maximum size of approx. 300 nm (cf. Gottselig et al., 2017b; section 2.6). Thus, all fractionated nanoparticles and fine colloids fell within the operationally defined "dissolved phase" (<0.45 µm; Marschner and Kalbitz, 2003 and references therein).

The findings showed that Field Flow Fractionation allows a more detailed analysis of colloid-bound elements that would otherwise be assigned to the term 'dissolved', based on their size being <0.45 µm. Only colloidal (1 nm to approx. 300 nm) elements were assessed, so that the discrepancy to the total elemental concentration in the samples then reflected the truly dissolved part. Our data showed that the portion of elements bound to colloids (here assessed as the sum of the three fractions) comprised 26.8 ± 16.5% (mean ± SD) of Al, 24.3 ± 24.0% of P, 22.3 ± 29.7% of Mn, and 55.0 ± 26.7% of Fe, while only 6.2 ± 10.8% of org C, 2.1 ± 7.4% of Si, and 3.9 ± 4.6% of Ca was bound to or within the colloids (cf. section 2.4). The percentages of org C in the colloids were thus of similar magnitude than those of Si and Ca, which was lower than previously reported (Gottselig et al., 2014; Gottselig et al., 2017a) but in line with previous measurements of stream water in the Conventwald (Gottselig et al., 2017b).

3.2 Spatial variability of nanoparticles and colloids

299 The above mentioned fractionation pattern occurred in all sample types and throughout the
300 whole sampling period (cf. Figure 2). Figure 2 displays fractograms of ICP-MS and OCD data
301 averaged for each sample type over the course of the 13 months. Raw data of ICP-MS
302 fractograms were drift corrected according to the internal standard Rh and both ICP-MS and
303 OCD data were baseline corrected prior to visualization. Between the different sample types,
304 the peak intensity varied between the fractions. The throughfall samples, for instance,
305 exhibited a dominance of particles < 20 nm occurring in the 1st fraction peak (Figure 2). In
306 contrast, the groundwater samples showed prominent signals of 20-60 nm sized particles in
307 the 2nd fraction (Figure 2), mostly dominated by the Ca signal. The peak patterns of two trench
308 samples (0-10 cm and 10-230 cm; Figure 2) closely resembled the throughfall samples (Figure
309 2). Hence, along the water transport pathway from throughfall to groundwater, NNPs were
310 partly replaced by larger particles, thus likely indicating a re-formation of the latter.

311 Apart from mere size and abundance, the elemental composition of NNP and larger colloids
312 may be indicative of their origin (Gottselig et al., 2017a). Here, the trench samples contained
313 mainly 1st fraction particles primarily consisting of org C, Al, Fe and Ca (Figure 2, Table 2). A
314 further resemblance was observed for the peak composition of all other sample types (cf.
315 Figure 2). Thus, rainwater, groundwater, trench 230-300 cm and the stream water exhibited
316 similar peak expression patterns and magnitudes (cf. Figure 2). Here, we primarily observed
317 2nd fraction particles consisting of Ca but also of P and Si and 3rd fraction particles with highest
318 average signals for org C, Si and P.

319 3.3 Yearly variation of nanoparticles and colloids

320 The colloidal concentrations of the stream water elements showed seasonal differences but
321 especially substantial concentration decreases in the months May to October after

multiplication with discharge (cf. Figure 3, left; supplementary information, Figure SI3). This decline also corresponded to seasonal fluctuations in precipitation amounts and soil moisture (cf. Figure 1, supplementary information, Figure SI2) and was reciprocal to the change of air and stream temperature and relative contribution of groundwater in the stream as determined through EMMA (cf. Figure 1; supplementary information Figure SI2).

The relative proportions of elements bound to a given colloid size fraction varied up to a factor of ~10, for example, for 3rd fraction Ca (cf. Figure 3, supplementary information, Figure SI3) over the season. Looking at P, a median range of 20.8% to 32.6% P within the 1st fraction, 27.1% to 39.7% P in the 2nd fraction and 29.3% to 43.4% P in the 3rd fraction relative to the total colloidal loads was found (factor ~2; cf. Figure 3, supplementary information, Figure SI4). The colloidal P load was lowest between April and October, yet with highest portions of P found in the largest colloids during this period (cf. Figure 3, supplementary information, Figure SI4). This seasonal trend was not only seen for P but also for colloidal Fe in groundwater samples (supplementary information, Figure SI4). Fe in rain and stream water as well as Al and Si in all sample types showed an opposing trend with an increase in 1st fraction Fe peaking around May at the expense of the 3rd fraction and at steady 2nd fraction concentrations (Figure 3; supplementary information, Figure SI4). Further noteworthy, Ca and Mn 1st fractions showed seasonal variations with peak concentrations around May at the expense of 2nd fraction and at similar 3rd fraction concentrations throughout the year (Figure 3; supplementary information, Figure SI4). Org C clearly dominated the 3rd fraction with the exception of some spring samples (supplementary information, Figure SI4) and the occurrence of 1st fraction org C in the throughfall, yet concentrations were often below detection limit and thus evident seasonal patterns could not be seen.

3.4 Predictability of colloidal elemental composition over the course of one year

346 To better understand seasonal effects on the occurrence of elements within NNP and fine
347 colloid fractions, we correlated fraction-specific elemental and total sample concentrations in
348 accordance to our former study on European scale (Gottselig et al., 2017a). For all samples of
349 the current study, we found that the concentrations of org C, Al, P, Ca, Mn and Fe within a
350 given size fraction correlated linearly with the total element concentration (Figure 4; Table 1).
351 In contrast, no linear correlation was found for colloidal Si, thus aggravating simple occurrence
352 predictions for the element Si (Table 1).

353 The same evaluations with only the stream water samples confirmed the linear relationship
354 for the $\log_{10}$ transformed Al, P and Fe concentration, which are the elements with largest
355 proportions of colloidal phases (section 3.1). In contrast, respective relationships for org C, Si,
356 Ca and Mn were rather scattered (Table 1, bottom). For org C this lacking relationship for the
357 stream water samples can most likely be attributed to the few data points available, whereas
358 for Ca the relationship found for all sample types was clearly absent when only considering
359 the stream water (cf. Table 1) because the precipitation data (rainwater and throughfall)
360 created the linearity (cf. Figure 5). Concerning P, the linear relationship was confirmed by the
361 stream water data and here also showed significant linear correlations for the 3rd fraction to
362 total P relationship.

363 3.5 Stream water composition

364 A comparison between sample types for the afore mentioned relationships can reflect
365 similarities in colloidal origin and thus allow to identify potential inflows into the stream.
366 Taking into consideration that larger sized colloids were detected in the rainwater after it
367 passed through the canopy (rainwater in comparison to throughfall), we investigated the
368 change in colloid elemental concentration in the aqueous samples and in comparison to WDC

extracted from the different soil horizons. As shown in Figure 5 for all elements, the chemical composition of stream and groundwater (and rainwater for Al and Fe) was similar.

The concentration bi-plots (Figure 5) also revealed that different sample types were characterized by different element loads, e.g. for Al, Mn and Fe, ground and stream water were found in the lowest concentration range of both total and colloidal element concentrations. Throughfall and rainwater samples clearly exhibited lowest concentrations in total Si and Ca, but not necessarily lower colloidal concentrations of these elements, respectively. In contrast, the trench samples clustered at elevated colloidal and total element loads of Al, P, Fe, and Mn. However, the chemical composition of WDC was not reflected by any aqueous sample (Figure 5). Thus, the WDC method potentially overestimates the actual element mobilization from soil profiles (Missong et al., 2018b).

The C-Q relationships revealed seven significant correlations (Pearson, $p<0.05$) out of which six were from 3rd fraction elemental concentrations. The only significant correlation of 2nd fraction concentrations with discharge was for P in catchment 1 weir at a slope of 0.57 with r^2=0.38. Further, for the 3rd fraction, org C showed significant correlations for catchment 1 spring (slope = -0.36, r^2 = 0.47) and weir (slope = -0.63, r^2 = 0.55) samples, Al for catchment 1 (slope = 0.55, r^2 = 0.60) and catchment 2 (slope = 0.51, r^2 = 0.67) weirs and Fe also for catchment 1 (slope = 0.34, r^2 = 0.45) and catchment 2 (slope = 0.54, r^2 = 0.67) weirs. Apparently, org C, Al and Fe guided the overall role of colloidal fluxes for the total element loss from the ecosystem.

3.6 Interdependency of elemental concentrations

There is a high probability to encounter multi-element particles in natural samples. Thus, Pearson correlations were calculated for all sample types to assess the co-transport of

392 different elements within one fraction and thus to infer that these elements occurred within
393 one particle in the fraction. Table 2 provides an overview over all significant ($p<0.05$) Pearson
394 correlation coefficients between elements of the respective fraction and sample type. All
395 sample types, excluding the trench, showed a low number of significant correlations. In
396 groundwater and rainwater samples, mainly correlations between Ca and Si as well as Fe and
397 Al were found; in the throughfall samples additionally org C particles associated to Al, P and/or
398 Fe occurred (cf. Table 2). The correlations of the trench samples included all trench depths
399 due to low sample numbers of especially the deepest trench collection (n=3; cf.
400 supplementary information, Table SI1). Here, especially for the 1st fraction many potential
401 particle compositions were detected with decreasing numbers as particle sizes increased (cf.
402 Table 2). Stream water results showed highest similarity to groundwater and rainwater
403 correlations (cf. Table 2).

404

405 4. Discussion

406 4.1 Relevance of natural nanoparticles and colloids in forest ecosystem compartments

407 The percentage of elements within the NNP and colloid fractions in relation to the total
408 elemental concentrations was used as a straightforward calculation to determine the
409 relevance of NNP and colloids in stream water. For the current study, the percentage of
410 elemental binding to NNP and colloids was substantial for Al, P, Mn and especially Fe with
411 average percentages between 22 and 55% (cf. section 3.1), thus confirming their steady
412 occurrence also in colloidal form despite the low overall particle concentrations in the stream
413 water (cf. supplementary information, Figure SI5). Yet, with the exception of Fe, Mn and Si,
414 the percentages were markedly lower than found for other stream waters (Dahlqvist et al.,

2004; Gottselig et al., 2017a; Hill and Aplin, 2001; Jarvie et al., 2012; Martin et al., 1995; Wen et al., 1999). Hill and Aplin (2001) and Jarvie et al. (2012), for instance, found average Al binding in riverine samples between 45 and 55%, thus exceeding our proportions by a factor of two. Also, studies on P in NNP and colloid fractions frequently reported binding percentages between 45 and 66% (Gottselig et al., 2017a; Jarvie et al., 2012; Missong et al., 2018b) in relation to 24% found here. The largest difference to other ecosystems was found for C, where we determined that NNP and colloids contributed to 6% of org C in solution, while other studies found binding percentages between 20 and 60% org C (Gottselig et al., 2017a; Jarvie et al., 2012; Martin et al., 1995; Wen et al., 1999). Nevertheless, the data agree with assessments on similar Conventwald stream samples (Gottselig et al., 2017b). Hence, we suggest that the lower proportion of elements bound to NNP and colloids relative to other studies reflects the specific flow pathways of this forest ecosystem, where a steep slope allows the generation of stream water without further seepage inputs from soil solutions.

Noteworthy, the elements detected in the NNP and fine colloid fractions occurred in three distinct size ranges (Gottselig et al., 2017a; Figure 2; see also Jiang et al., 2015; Missong et al., 2016), and not solely as particles <25 nm as reported by Dahlqvist et al. (2004) and Andersson et al. (2006). The contribution of these fractions to total element loads varied but were, at least in part, also specific for a given sample compartment. Throughfall and soil leachates integrating from 0 to 2.3 m of soil showed a dominance of the 1st fraction peak, i.e., of particles <20 nm. Rainwater, deep trench samples and stream water showed the occurrence of all peaks (Figure 2), but with different P/Ca ratio in comparison to the groundwater samples. This finding indicates different mixing processes in the ecosystem. Throughfall, which also received additional org C from the canopy (Figure 2), likely infiltrated the soil rapidly and maintained its NNP and fine colloidal signature down to 2.3 m depth. Soil leachate from >2.3 m depth

showed some groundwater contribution. Rainwater may have influenced the stream's chemical composition, but due to the low areal extension of the streams a dominating impact seems unlikely. The rainwater input largely showed similarities to groundwater, which likely feeds the stream.

Not all findings can be explained by mixing processes. The lacking dominance of the small NNP <20 nm in the groundwater as compared with throughfall, for instance, suggests that also during water partitioning in the ecosystem NNP and larger colloids are dynamic. Particularly the larger, Ca-rich particles in the size range of 20-60 nm must have reformed in the ecosystem and cannot merely stem from leaching inputs. The underlying kinetics of NNP breakdown and re-aggregation remain poorly constraint; yet, they must occur at annual scale to justify the seasonal patterns.

4.2 Seasonal patterns

Microclimate is usually considered as one main driver of the seasonality in element fluxes (e.g. Foster and Bhatti, 2006). Elemental loads in catchment 1 and 2 weirs fluctuated reciprocal to air and thus stream water temperature and stream water electrical conductivity but parallel to soil moisture and precipitation (Figure 1 and 3; supplementary information, Figure SI1). These fluctuations were most pronounced between summer and winter. Indeed, total colloidal elemental concentrations were substantially lower in summer than in winter. This trend was also observed in other ecosystems, e.g., for Ca in particles <0.22 µm in an arctic river where the respective concentrations declined almost 4-fold from winter to summer loads, with substantial dilution occurring due to the spring flood (cf. Dahlqvist et al., 2004). In our study, no distinct spring flood event occurred from multiple rainfall or snowmelt events (supplementary information, Figure SI2), yet, due to lower discharge and thus water amounts

462 in the ecosystem in summer months, the colloidal elemental loads decreased accordingly (e.g.
463 Figure 3).

464 Intriguingly, different elements responded differently to this seasonal trend. For example, the
465 colloidal P concentrations showed a maximum in February and March in both stream and
466 groundwater, whereas colloidal Ca concentrations increased after July (supplementary
467 information, Figure SI5). These differences reflect the different sources of the elements. While
468 P is hardly leached (Bol et al., 2016) and thus likely stemmed from surface runoff (Heathwaite
469 and Dils, 2000), the occurrence of a deep layer rich in easily exchangeable Ca (Uhlig and von
470 Blanckenburg, 2019) fed groundwater and explained the elevated P/Ca ratios therein (Figure
471 2). Hence, the dynamics of colloidal P differed from the groundwater coupled dynamics of Ca.

472 Existing or lacking correlations on the variability between the binding percentages of the
473 different NNP and colloid fractions provide insight into seasonal changes between the particle
474 fractions (Figure 3; supplementary information, Figure SI3 and SI4). In this regard, the
475 dynamics of Fe and Al as well as of org C and P were closely coupled while that of other
476 elements were not (Table 2), also reflecting their different contribution to overall colloid loads.

477 Through an assessment of fraction concentrations of multiple German streams including the
478 Conventwald, Gottselig et al. (2017b) determined building block elements of 1st fraction NNP
479 to be metals or org C, while 2nd fraction NNP identified as Fe-org C or metal particles and 3rd
480 fraction NNP and colloids largely were found to be clay minerals and/or larger Fe-org C
481 compounds. Fe as micronutrient and fundamental constituent of all three fractions shows a
482 clear seasonality within the 1st fraction (<20 nm NNP) with minimal occurrence in stream
483 waters in November and maxima in March and June (Figure 3). These trends may be
484 interpreted in terms of a nutrient depletion in November following the growth and

development period of the plants, and an enrichment when biogeochemical weathering rates are high towards end of spring (Yesavage et al., 2012). Moreover, the occurrence of Fe in the 1st fraction seems to have a reciprocal effect on the 3rd fraction, suggesting that different colloidal sizes are linked via input and aggregation processes, for instance.

Org C often correlates well with Fe in micrometer sized particles (e.g. Gandois et al., 2010; Gottselig et al., 2017b) and can be indicative of soil runoff (McIntosh et al., 2017). Yet, org C showed lower concentrations in Conventwald stream water (supplementary information, Figure SI3 and SI4) in comparison to earlier findings (Gottselig et al., 2017b; Jarvie et al., 2012; Martin et al., 1995; Wen et al., 1999). Single higher concentrations were detected in throughfall in May (0.4 mmol L^{-1}) and in soil leachate samples of September and October (0-10 cm, 0.6 and 0.7 mmol L^{-1}; data not shown). However, these finding apparently do not influence org C concentrations in stream water particles. Thus, no seasonality of org C was found. The same was true for the major components of clay minerals (Al and Si), a typical component of 3rd fraction stream water particles.

A further element generally not in focus in the context of P in slightly acidic forest catchments but which showed high concentrations in all three stream water particle fractions and high binding percentages in the 2nd fraction was Ca (Figure 1 and 3). As previously discussed by Missong et al. (2018b), Ca seems to be a further important building block structure, especially in the context of P, and potentially even independent of pH. Despite a siliceous bedrock, a constant layer rich in exchangeable Ca which is also hydrologically connected to the stream must be present due to the high concentrations in stream and groundwater as well as trench samples (cf. Figure 5), as well as the constant binding percentages in all three fractions with only slight effect of seasonality (Figure 3). In fact, this layer was found in the deep subsoil beneath ~3 m depth (Uhlig and von Blanckenburg, 2019). Hence, even if surface soils are

509 acidified, it may be essential to include Ca in the analysis of building block structures of NNP
510 and fine colloids in acidic forest ecosystems.

511 4.3 Stream water inflows and further influential parameters

512 The origin of particles in stream waters can be traced through assessment of a combination
513 of hydrological dynamics, elemental reaction to changes in discharge as well as indicator
514 elements of different flow pathways. Pokrovsky et al. (2010) distinguished their data according
515 to dynamics based on two inflows into stream water: i) groundwater poor in organic matter
516 but high in truly dissolved species released from the bedrock, and ii) shallow soil waters rich
517 in organics and thus NNP and colloids. Figure 5 indicates that the majority of water entering
518 the stream must be derived from groundwater and showed additional occasional similarities
519 to subsoil (>2.3 m) trench collection, which were most probably also mainly influenced by
520 groundwater. Following the classification introduced by Pokrovsky et al. (2010), these findings
521 imply that the influence of shallow soil water was minimal in stream waters of the
522 Conventwald due to the juxtaposition of stream and groundwater to data from the upper
523 trench collection (<2.3 m) and soil pits (Figure 5; Lang et al., 2017; Missong et al., 2018a).

524 A further observation from the plots of Figure 5 is the gradual variation from aqueous sample
525 concentrations to the data from the soil pits. Particularly for Fe and Al, but also for org C, P
526 and Mn, the NNP and fine colloid concentrations seem to represent a sub-fraction of the
527 concentrations derived for WDC (Missong et al., 2018a). In contrast, Ca shows enrichment in
528 NNP and fine colloids at similar total Ca concentrations (Figure 5). In no case the
529 concentrations of WDC were reached in aqueous colloids, suggesting that the former may only
530 indicate nutrient mobilization far off from realistic colloidal concentration ranges detected in
531 the latter.

The C-Q relationships revealed that an increase in discharge has a significant enrichment effect only for P in 2nd fraction particles and Al and Fe in 3rd fraction particles, whereas, in contrast, org C concentrations decline with increasing discharge (cf. section 3.4). This finding was indicative of a dominant non-surface water source entering the stream at high discharge, due to the dilutive C-Q behavior for org C, which was additionally rich in Ca and Si (Figure 5).

5. Conclusions

The assessment of natural nanoparticles and colloids in multiple aqueous compartments of a forest ecosystem over the course of one year by means of Field Flow Fractionation has revealed that these natural particles occur throughout the year in the analyzed water compartments. Judging from the fractograms, rainwater, stream water and groundwater contained similar particle distributions and throughfall and soil leachates. Nevertheless, the elemental loads varied with higher values in winter than in summer. Intriguingly, this variation only affected one size class per element and sample while at least one of the three fractions (per element) was fairly stable throughout the whole year. The seasonal occurrence of NNP and colloids is thus not only affected by seasonal variations in water fluxes but also by seasonal dynamics in particle reformation by dispersion, aggregation, and mixing with different elements.

Different elements bound to NNP and colloids partly originated from different sources. While P mainly stemmed from processes at the terrestrial land surface, the origin of Ca was clearly related to interactions in the groundwater aquifer. As a result, the seasonal dynamics of these different colloidal element loads were not immediately coupled and resulted, thus, in different

element ratios of, e.g., P/Ca in throughfall and soil leachates compared to ground- and stream water, respectively.

Acknowledgements

The authors thank the student assistants of the Chair of Hydrology, Freiburg for their assistance in sample collection and data recording. This work was partially funded by DFG KL 2495/1-1 and DFG GO 2899/1-1 and conducted in the framework of the SPP 1685 of the German Research Foundation.

References

Andersson, K., Dahlqvist, R., Turner, D., Stolpe, B., Larsson, T., Ingri, J., Andersson, P., 2006. Colloidal rare earth elements in a boreal river: Changing sources and distributions during the spring flood. Geochim. Cosmochim. Acta 70, 3261–3274. https://doi.org/10.1016/j.gca.2006.04.021.

Baalousha, M., Stolpe, B., Lead, J.R., 2011. Flow field-flow fractionation for the analysis and characterization of natural colloids and manufactured nanoparticles in environmental systems: A critical review. J. Chroma. A 1218, 4078–4103. https://doi.org/10.1016/j.chroma.2011.04.063.

Baik, M.-H., Yun, J.-I., Bouby, M., Hahn, P.-S., Kim, J.-I., 2007. Characterization of aquatic groundwater colloids by a laser-induced breakdown detection and ICP-MS combined with an asymmetric flow field-flow fractionation. Korean J. Chem. Eng. 24, 723–729. https://doi.org/10.1007/s11814-007-0033-7.

Baken, S., Moens, C., van der Grift, B., Smolders, E., 2016a. Phosphate binding by natural iron-rich colloids in streams. Water Res. 98, 326–333. https://doi.org/10.1016/j.watres.2016.04.032.

Baken, S., Regelink, I.C., Comans, R.N.J., Smolders, E., Koopmans, G.F., 2016b. Iron-rich colloids as carriers of phosphorus in streams: A field-flow fractionation study. Water Res. 99, 83–90. https://doi.org/10.1016/j.watres.2016.04.060.

Barthold, F.K., Tyralla, C., Schneider, K., Vaché, K.B., Frede, H.-G., Breuer, L., 2011. How many tracers do we need for end member mixing analysis (EMMA)? A sensitivity analysis. Water Resour. Res. 47. https://doi.org/10.1029/2011WR010604.

Bol, R., Julich, D., Brödlin, D., Siemens, J., Kaiser, K., Dippold, M.A., Spielvogel, S., Zilla, T., Mewes, D., Blanckenburg, F. von, Puhlmann, H., Holzmann, S., Weiler, M., Amelung, W., Lang, F., Kuzyakov, Y., Feger, K.-H., Gottselig, N., Klumpp, E., Missong, A., Winkelmann, C., Uhlig, D., Sohrt, J., Wilpert, K.v., Wu, B., Hagedorn, F., 2016. Dissolved and colloidal phosphorus fluxes in forest ecosystems—an almost blind spot in ecosystem research. J. Plant Nutr. Soil Sci. 179, 425–438. https://doi.org/10.1002/jpln.201600079.

Buffle, J., Leppard, G.G., 1995. Characterization of aquatic colloids and macromolecules. 2. Key role of physical structures on analytical results. Environ. Sci. Technol. 29, 2176–2184. https://doi.org/10.1021/es00009a005.

Cizdziel, J.V., Guo, C., Steinberg, S.M., Yu, Z., Johannesson, K.H., 2008. Chemical and colloidal analyses of natural seep water collected from the exploratory studies facility inside Yucca Mountain, Nevada, USA. Environ. Geochem. Health 30, 31–44. https://doi.org/10.1007/s10653-007-9105-1.

Dahlqvist, R., Andersson, K., Ingri, J., Larsson, T., Stolpe, B., Turner, D., 2007. Temporal variations of colloidal carrier phases and associated trace elements in a boreal river. Geochim. Cosmochim. Acta 71, 5339–5354. https://doi.org/10.1016/j.gca.2007.09.016.

Dahlqvist, R., Benedetti, M.F., Andersson, K., Turner, D., Larsson, T., Stolpe, B., Ingri, J., 2004. Association of calcium with colloidal particles and speciation of calcium in the Kalix and Amazon rivers. Geochim. Cosmochim. Acta 68, 4059–4075. https://doi.org/10.1016/j.gca.2004.04.007.

Degueldre, C., Triay, I., Kim, J.-I., Vilks, P., Laaksoharju, M., Miekeley, N., 2000. Groundwater colloid properties: A global approach. Appl. Geochem. 15, 1043–1051. https://doi.org/10.1016/S0883-2927(99)00102-X.

Dietze, M., Dietze, E., 2013. EMMAgeo: End-member modelling algorithm and supporting functions for grain-size analysis. R package version 0.9 1.

Erickson, H.P., 2009. Size and shape of protein molecules at the nanometer level determined by sedimentation, gel filtration, and electron microscopy. Biol. Proced. Online 11, 32–51. https://doi.org/10.1007/s12575-009-9008-x.

Fernández-Martínez, M., Vicca, S., Janssens, I.A., Sardans, J., Luyssaert, S., Campioli, M., Chapin Iii, F.S., Ciais, P., Malhi, Y., Obersteiner, M., Papale, D., Piao, S.L., Reichstein, M., Roda, F., Penuelas, J., 2014. Nutrient availability as the key regulator of global forest carbon balance. Nat. Clim. Chang. 4, 471–476. https://doi.org/10.1038/nclimate2177.

Foster, N.W., Bhatti, J.S., 2006. Forest ecosystems: Nutrient cycling. Encyclopedia of soil science. New York: Taylor & Francis Group, 718–721.

Frisbee, M.D., Phillips, F.M., Campbell, A.R., Liu, F., Sanchez, S.A., 2011. Streamflow generation in a large, alpine watershed in the southern Rocky Mountains of Colorado: Is streamflow generation simply the aggregation of hillslope runoff responses? Water Resour. Res. 47. https://doi.org/10.1029/2010WR009391.

Gandois, L., Tipping, E., Dumat, C., Probst, A., 2010. Canopy influence on trace metal atmospheric inputs on forest ecosystems: Speciation in throughfall. Atmos. Environ. 44, 824–833. https://doi.org/10.1016/j.atmosenv.2009.11.028.

Gottselig, N., Amelung, W., Kirchner, J.W., Bol, R., Eugster, W., Granger, S.J., Hernández-Crespo, C., Herrmann, F., Keizer, J.J., Korkiakoski, M., Laudon, H., Lehner, I., Loefgren, S., Lohila, A., Macleod, C.J.A., Moelder, M., Mueller, C., Nasta, P., Nischwitz, V., Paul-Limoges, E., Pierret, M.-C., Pilegaard, K., Romano, N., Sebastià, M.-T., Staehli, M., Voltz, M., Vereecken, H., Siemens, J., Klumpp, E., 2017a. Elemental composition of natural nanoparticles and fine colloids in European forest stream waters and their role as phosphorus carriers. Global Biogeochem. Cycles 31, 1592–1607. https://doi.org/10.1002/2017GB005657.

Gottselig, N., Bol, R., Nischwitz, V., Vereecken, H., Amelung, W., Klumpp, E., 2014. Distribution of phosphorus-containing fine colloids and nanoparticles in stream water of a forest catchment. Vadose Zone J. 13. https://doi.org/10.2136/vzj2014.01.0005.

Gottselig, N., Nischwitz, V., Meyn, T., Amelung, W., Bol, R., Halle, C., Vereecken, H., Siemens, J., Klumpp, E., 2017b. Phosphorus binding to nanoparticles and colloids in forest stream waters. Vadose Zone J. 16. https://doi.org/10.2136/vzj2016.07.0064.

Guinn Garrett, C., Vulava, V.M., Callahan, T.J., Jones, M.L., 2012. Groundwater–surface water interactions in a lowland watershed: Source contribution to stream flow. Hydrol. Process. 26, 3195–3206. https://doi.org/10.1002/hyp.8257.

Hart, B.T., Douglas, G.B., Beckett, R., Vanput, A., Vangrieken, R.E., 1993. Characterization of colloidal and particulate matter transported by the Magela Creek system, Northern Australia. Hydrol. Process. 7, 105–118. https://doi.org/10.1002/hyp.3360070111.

Hartland, A., Lead, J.R., Slaveykova, V., O'Carroll, D., Valsami-Jones, E., 2013. The Environmental Significance of Natural Nanoparticles. Nature Education Knowledge 4.

Haygarth, P., Turner, B.L., Fraser, A., Jarvis, S., Harrod, T., Nash, D., Halliwell, D., Page, T., Beven, K., 2004. Temporal variability in phosphorus transfers: Classifying concentration? discharge event dynamics. Hydrol. Earth Sys. Sci. Disc. 8, 88–97. https://hal.archives-ouvertes.fr/hal-00304795.

Haygarth, P.M., Warwick, M.S., House, W.A., 1997. Size distribution of colloidal molybdate reactive phosphorus in river waters and soil solution. Water Res. 31, 439–448. https://doi.org/10.1016/S0043-1354(96)00270-9.

Heathwaite, A.L., Dils, R.M., 2000. Characterising phosphorus loss in surface and subsurface hydrological pathways. Sci. Total Environ. 251, 523–538. https://doi.org/10.1016/s0048-9697(00)00393-4.

Herndon, E.M., Dere, A.L., Sullivan, P.L., Norris, D., Reynolds, B., Brantley, S.L., 2015. Landscape heterogeneity drives contrasting concentration–discharge relationships in shale headwater catchments. Hydrol. Earth Syst. Sci. 19, 3333–3347. https://doi.org/10.5194/hess-19-3333-2015.

Hill, D.M., Aplin, A.C., 2001. Role of colloids and fine particles in the transport of metals in rivers draining carbonate and silicate terrains. Limnol. Oceanogr. 46, 331–344. https://doi.org/10.4319/lo.2001.46.2.0331.

IUSS, 2015. World reference base for soil resources 2014, update 2015. International soil classification system for naming soils and creating legends for soil maps. World Soil Resources Reports 106.

Jarvie, H.P., Neal, C., Rowland, A.P., Neal, M., Morris, P.N., Lead, J.R., Lawlor, A.J., Woods, C., Vincent, C., Guyatt, H., Hockenhull, K., 2012. Role of riverine colloids in macronutrient and metal partitioning and transport, along an upland-lowland land-use continuum, under low-flow conditions. Sci. Total Environ. 434, 171–185. https://doi.org/10.1016/j.scitotenv.2011.11.061.

Jiang, X., Bol, R., Nischwitz, V., Siebers, N., Willbold, S., Vereecken, H., Amelung, W., Klumpp, E., 2015. Phosphorus Containing Water Dispersible Nanoparticles in Arable Soil. J. Environ. Qual. 44, 1772–1781. https://doi.org/10.2134/jeq2015.02.0085.

Lang, F., Krüger, J., Amelung, W., Willbold, S., Frossard, E., Bünemann, E.K., Bauhus, J., Nitschke, R., Kandeler, E., Marhan, S., 2017. Soil phosphorus supply controls P nutrition strategies of beech forest ecosystems in Central Europe. Biogeochem. 136, 5–29. https://doi.org/10.1007/s10533-017-0375-0.

Lorenz, M., 1995. International co-operative programme on assessment and monitoring of air pollution effects on forests-ICP forests. Water Air Soil Pollut. 85, 1221–1226. https://doi.org/10.1007/BF00477148.

Maher, K., 2011. The role of fluid residence time and topographic scales in determining chemical fluxes from landscapes. Earth Planet. Sci. Lett. 312, 48–58. https://doi.org/10.1016/j.epsl.2011.09.040.

Marschner, B., Kalbitz, K., 2003. Controls of bioavailability and biodegradability of dissolved organic matter in soils. Geoderma 113, 211–235. https://doi.org/10.1016/s0016-7061(02)00362-2.

Martin, J.M., Dai, M.H., Cauwet, G., 1995. Significance of colloids in the biogeochemical cycling of organic-carbon and trace-metals in the Venice lagoon (Italy). Limnol. Oceanogr. 40, 119–131. https://doi.org/10.4319/lo.1995.40.1.0119.

McIntosh, J.C., Schaumberg, C., Perdrial, J., Harpold, A., Vázquez-Ortega, A., Rasmussen, C., Vinson, D., Zapata-Rios, X., Brooks, P.D., Meixner, T., 2017. Geochemical evolution of the Critical Zone across variable time scales informs concentration-discharge relationships: Jemez River Basin Critical Zone Observatory. Water Resour. Res. 53, 4169–4196. https://doi.org/10.1002/2016WR019712.

Missong, A., Bol, R., Nischwitz, V., Krüger, J., Lang, F., Siemens, J., Klumpp, E., 2018a. Phosphorus in water dispersible-colloids of forest soil profiles. Plant Soil 427, 71–86. https://doi.org/10.1007/s11104-017-3430-7.

Missong, A., Bol, R., Willbold, S., Siemens, J., Klumpp, E., 2016. Phosphorus forms in forest soil colloids as revealed by liquid-state 31P-NMR. J. Plant Nutr. Soil Sci. 179, 159–167. https://doi.org/10.1002/jpln.201500119.

690 Missong, A., Holzmann, S., Bol, R., Nischwitz, V., Puhlmann, H., Wilpert, K.v., Siemens, J., Klumpp, E.,
691 2018b. Leaching of natural colloids from forest topsoils and their relevance for phosphorus
692 mobility. Sci. Total Environ. 634, 305–315. https://doi.org/10.1016/j.scitotenv.2018.03.265.

693 Neubauer, E., Köhler, S.J., Kammer, F. von der, Laudon, H., Hofmann, T., 2013. Effect of pH and Stream
694 Order on Iron and Arsenic Speciation in Boreal Catchments. Environ. Sci. Technol. 47, 7120–7128.
695 https://doi.org/10.1021/es401193j.

696 Nischwitz, V., Gottselig, N., Missong, A., Klumpp, E., Braun, M., 2018. Extending the capabilities of field
697 flow fractionation online with ICP-MS for the determination of particulate carbon in latex and
698 charcoal. J. Anal. Atomic Spectr. 33, 1363–1371. https://doi.org/10.1039/C8JA00101D.

699 Perdrial, J.N., McIntosh, J., Harpold, A., Brooks, P.D., Zapata-Rios, X., Ray, J., Meixner, T., Kanduc, T.,
700 Litvak, M., Troch, P.A., 2014. Stream water carbon controls in seasonally snow-covered mountain
701 catchments: Impact of inter-annual variability of water fluxes, catchment aspect and seasonal
702 processes. Biogeochem. 118, 273–290. https://doi.org/10.1007/s10533-013-9929-y.

703 Perry, D.A., Oren, R., Hart, S.C. 14.4 Chemical Properties of Soils. In: Forest ecosystems: JHU Press;
704 2008. p. 269–281.

705 Pokrovsky, O.S., Viers, J., Shirokova, L.S., Shevchenko, V.P., Filipov, A.S., Dupré, B., 2010. Dissolved,
706 suspended, and colloidal fluxes of organic carbon, major and trace elements in the Severnaya Dvina
707 River and its tributary. Chem. Geol. 273, 136–149.
708 https://doi.org/10.1016/j.chemgeo.2010.02.018.

709 Ranville, J.F., Macalady, D.L. Natural organic matter in catchments. In: Saether OM, Caritat P de,
710 editors. Geochemical processes, weathering and groundwater recharge in catchments; 1997. p.
711 263–303.

712 Regelink, I.C., Koopmans, G.F., van der Salm, C., Weng, L., van Riemsdijk, W.H., 2013. Characterization
713 of Colloidal Phosphorus Species in Drainage Waters from a Clay Soil Using Asymmetric Flow Field-
714 Flow Fractionation. J. Environ. Qual. 42, 464–473. https://doi.org/10.2134/jeq2012.0322.

715 Regelink, I.C., Voegelin, A., Weng, L.P., Koopmans, G.F., Comans, R.N.J., 2014. Characterization of
716 Colloidal Fe from Soils Using Field-Flow Fractionation and Fe K-Edge X-ray Absorption
717 Spectroscopy. Environ. Sci. Technol. 48, 4307–4316. https://doi.org/10.1021/es405330x.

718 Rosenthal, E., 1987. Chemical composition of rainfall and groundwater in recharge areas of the Bet
719 Shean-Harod multiple aquifer system, Israel. J. Hydrol. 89, 329–352. https://doi.org/10.1016/0022-
720 1694(87)90185-5.

721 Saito, T., Hamamoto, T., Mizuno, T., Iwatsuki, T., Tanaka, S., 2015. Comparative study of granitic and
722 sedimentary groundwater colloids by flow-field flow fractionation coupled with ICP-MS. J. Anal.
723 Atomic Spectr. 30, 1229–1236. https://doi.org/10.1039/C5JA00088B.

724 Six, J., Elliott, E.T., Paustian, K., 1999. Aggregate and soil organic matter dynamics under conventional
725 and no-tillage systems. Soil Sci. Soc. Am. J. 63, 1350–1358.
726 https://doi.org/10.2136/sssaj1999.6351350x.

727 Sohrt J., 2019. Cycling of Phosphorus in Temperate Forested Hillslopes. Dissertation, Albert-Ludwigs-
728 Universität Freiburg.

729 Trostle, K.D., Ray Runyon, J., Pohlmann, M.A., Redfield, S.E., Pelletier, J., McIntosh, J., Chorover, J.,
730 2016. Colloids and organic matter complexation control trace metal concentration-discharge
731 relationships in Marshall Gulch stream waters. Water Resour. Res. 52, 7931–7944.
732 https://doi.org/10.1002/2016WR019072.

733 Uhlig, D., von Blanckenburg, F., 2019. How slow rock weathering balances nutrient loss during fast
734 forest floor turnover in montane, temperate forest ecosystems. Front. Earth Sci. 7, 159.
735 https://doi.org/10.3389/feart.2019.00159.

736 Vries, W. de, Reinds, G.J., Vel, E., 2003. Intensive monitoring of forest ecosystems in Europe: 2:
737 Atmospheric deposition and its impacts on soil solution chemistry. For. Ecol. Manage. 174, 97–115.
738 https://doi.org/10.1016/S0378-1127(02)00030-0.

739 Wen, L.S., Santschi, P., Gill, G., Paternostro, C., 1999. Estuarine trace metal distributions in Galveston
740 Bay: importance of colloidal forms in the speciation of the dissolved phase. Mar. Chem. 63, 185–
741 212. https://doi.org/10.1016/s0304-4203(98)00062-0.

742 Yesavage, T., Fantle, M.S., Vervoort, J., Mathur, R., Jin, L., Liermann, L.J., Brantley, S.L., 2012. Fe cycling
743 in the Shale Hills Critical Zone Observatory, Pennsylvania: An analysis of biogeochemical
744 weathering and Fe isotope fractionation. Geochim. Cosmochim. Acta 99, 18–38.
745 https://doi.org/10.1016/j.gca.2012.09.029.

746

*Table 1: Top: Relations of fraction to total concentrations across all samples taken. Si: Fraction-specific median and percentage of fraction specific Si relative to all colloidal Si; org C, Al, P, Mn, Fe: Fraction-specific as function of total sample concentrations, linear regression slope (m) and intercepts (b) of log_{10} transformed data. n = 47; bottom: Relations of fraction to total concentrations across all stream water samples taken. Si, org C, Ca, Mn: Fraction-specific median and percentage of fraction specific relative to all colloidal concentrations; Al, P, Fe: Fraction-specific as function of total sample concentrations, linear regression slope (m) and intercepts (b) of log_{10} transformed data. n = 21; unit: µmol/L, org C: mmol/L; asterix: significant linear correlations (Pearson correlation, p<0.05). If elements are marked with * all data in the corresponding columns is significantly correlated, otherwise m and b are marked.*

all aqueous samples

	Si		org C		Al*		P*		Ca*		Mn*		Fe*	
fraction	*median*	*%all part.*	*m*	*b*	*m*	*b*	*m*	*b*	*m*	*b*	*m*	*b*	*m*	*b*
1st	0.06	30.4	0.40	-1.80	0.75	-1.33	0.35	-1.53	0.33	-0.75	0.46	-2.22	0.63	-1.32
2nd	0.07	35.8	2.43	-1.14	0.78	-1.65	0.28	-1.62	0.42	-0.60	0.18	-2.31	0.41	-1.63
3rd	0.04	33.8	1.72*	-1.58*	0.46	-1.58	0.24	-1.44	0.62	-1.97	0.13	-3.06	0.21	-1.80
all	0.11		2.40*	-0.82*	0.70	-0.91	0.30	-1.02	0.42	-0.40	0.26	-1.92	0.49	-0.94

stream water samples

	Si		org C		Ca		Mn		Al		P		Fe	
fraction	*median*	*%all part.*	*median*	*%all part.*	*median*	*%all part.*	*median*	*%all part.*	*m*	*b*	*m*	*b*	*m*	*b*
1st	0.08	31.4	0.005	23.8	0.68	27.1	0.0004	17.7	0.28	-1.57	0.32*	-1.62*	0.08	-2.20
2nd	0.06	35.9			1.57	63.5	0.0016	69.4	1.06	-1.35	0.52	-1.65	-0.01	-2.31
3rd	0.04	32.8	0.002	76.2	0.25	9.9	0.0004	15.7	0.86*	-1.24*	0.29*	-1.55*	0.72*	-0.93*
all	0.10		0.004		2.40		0.0024		0.61*	-0.91*	0.33*	-1.12*	0.36*	-1.13*

Table 2: Significant Pearson correlation coefficients ($p<0.05$) between the different measured elements per sample type and over all samples types and per fraction. Calculations were performed with log_{10} transformed data.

rainwater

1st fraction	Al	Si	P	Ca	Mn	Fe
Al						0.82
Si				0.73		

2nd fraction	Al	Si	P	Ca	Mn	Fe
Al		-0.90				
Si				0.89		
Ca					0.74	

throughfall

1st fraction	Al	Si	P	Ca	Mn	Fe
orgC	0.98		0.96			0.95
Al				0.71		0.97

trench

1st fraction	Al	Si	P	Ca	Mn	Fe
orgC			0.61	0.75	0.72	0.73
Al		0.77	0.75	0.75	0.75	0.94
Si				0.84	0.80	0.82
P				0.68	0.69	0.83
Ca					0.98	0.89
Mn						0.88

2nd fraction	Al	Si	P	Ca	Mn	Fe
Al		0.74		0.56	0.57	0.92
Si				0.67	0.59	0.75
P						0.63
Ca					0.94	0.69
Mn						0.71

3rd fraction	Al	Si	P	Ca	Mn	Fe
Al		0.75				0.97
Si					0.90	0.82

groundwater

1st fraction	Al	Si	P	Ca	Mn	Fe
Si				0.79		
P				-0.79		

3rd fraction	Al	Si	P	Ca	Mn	Fe
Al						0.69
P				-0.65		

stream water

1st fraction	Al	Si	P	Ca	Mn	Fe
orgC			0.85			
Al						0.60
Si			-0.62	0.78		
P				-0.76		

2nd fraction	Al	Si	P	Ca	Mn	Fe
Al						0.44
Si			-0.69	0.46		
P				-0.51		

3rd fraction	Al	Si	P	Ca	Mn	Fe
Al					0.36	0.73
P				-0.53		

all sample types

1st fraction	Al	Si	P	Ca	Mn	Fe
orgC	0.64	0.53	0.69	0.66	0.64	0.75
Al		0.39	0.40	0.53	0.56	0.89
Si				0.68	0.32	0.40
P					0.47	0.55
Ca					0.33	0.50
Mn						0.68

2nd fraction	Al	Si	P	Ca	Mn	Fe
orgC					0.69	
Al			0.30		0.33	0.78
Si				0.38		0.32
P				-0.33		0.43
Ca					0.28	0.31
Mn						0.45

3rd fraction	Al	Si	P	Ca	Mn	Fe
orgC	0.37		0.43			0.38
Al		0.55	0.45		0.40	0.82
Si					0.63	0.58
P				-0.31		0.36
Ca						
Mn						0.45

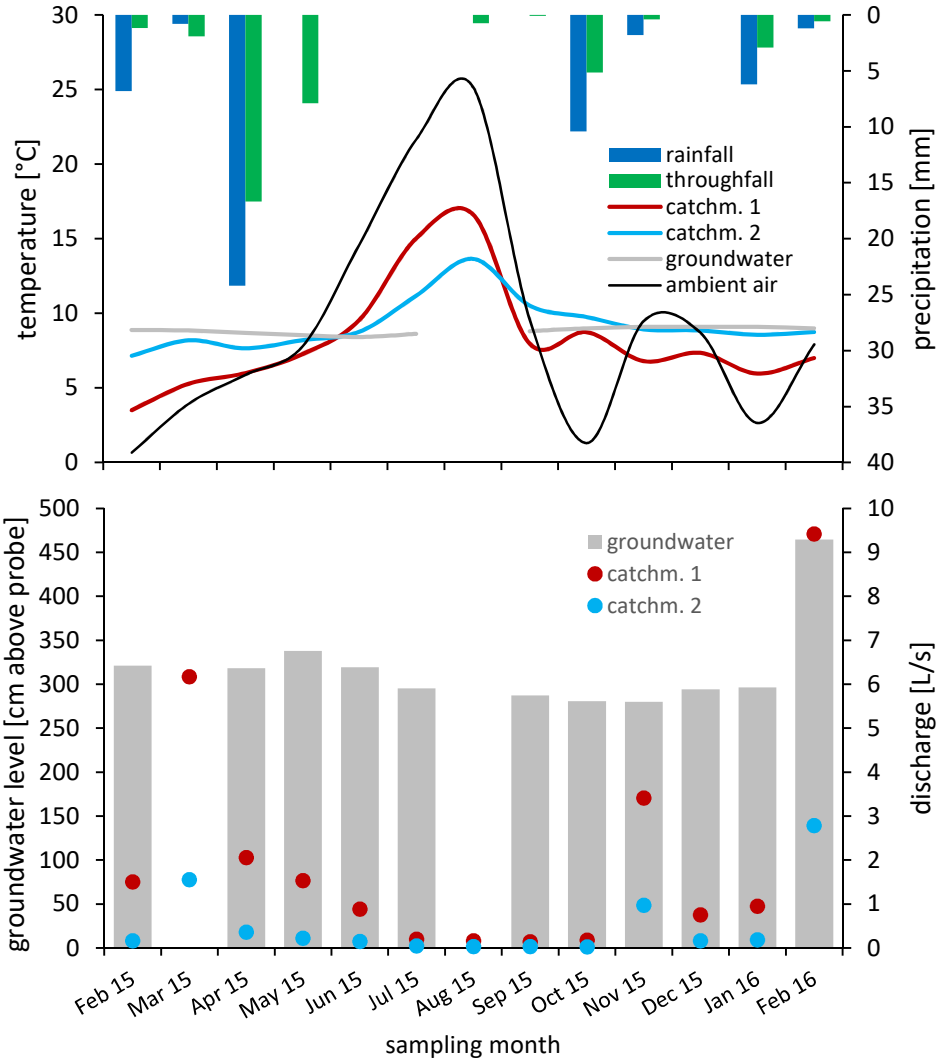

Figure 1: Hydrological and meteorological parameters recorded during the sampling period. Top: Temperature measured in stream water at both catchments, in groundwater and in the air as well as precipitation above and below tree canopy, Bottom: Average daily discharge at both catchments and groundwater level. Catchm. = catchment.

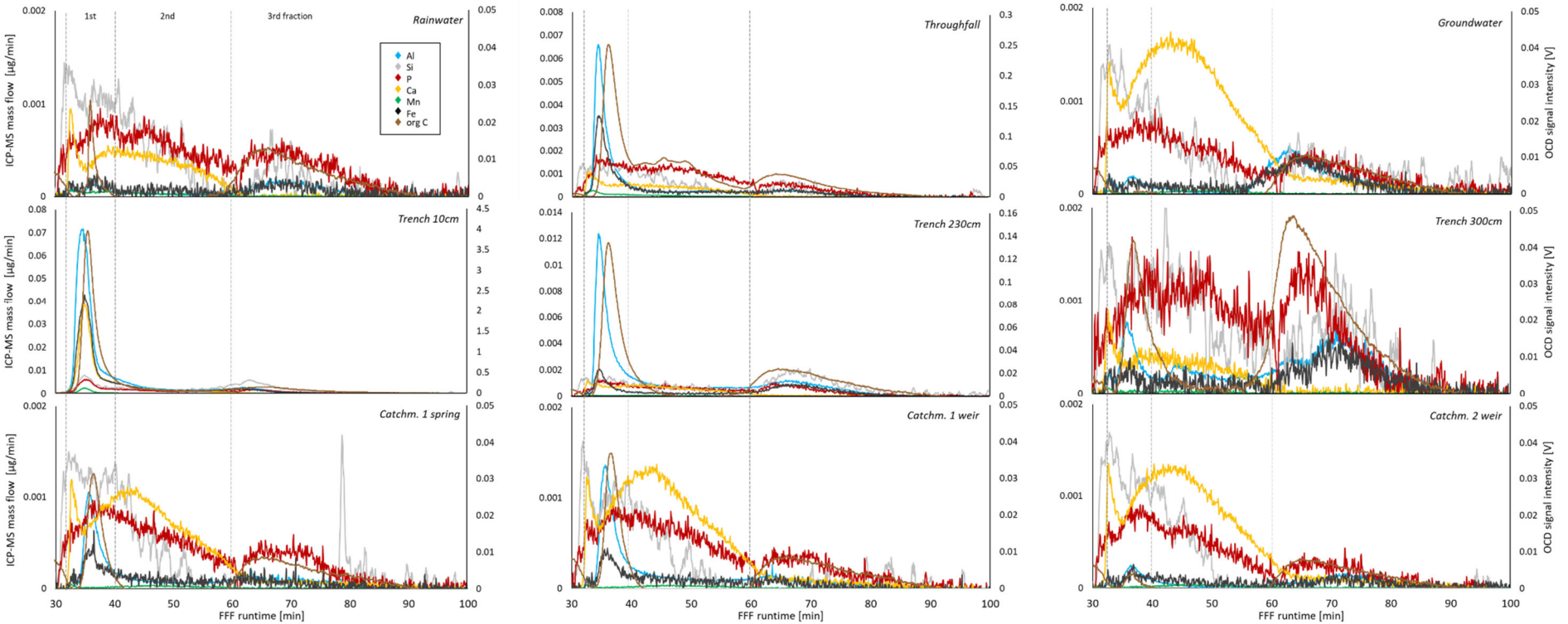

Figure 2: Fractograms of Asymmetric Flow Field Flow Fractionation coupled to ICP-MS and OCD. Data averaged over all samples taken per sample ICP-MS data: drift correction through internal standard Rh and baseline corrected, OCD data: baseline corrected prior to visualization. Note the different scaling of the y-axes. X-axes shortened, thus focus time not shown. Dotted lines separate the different fractions. Catchm. = catchment.

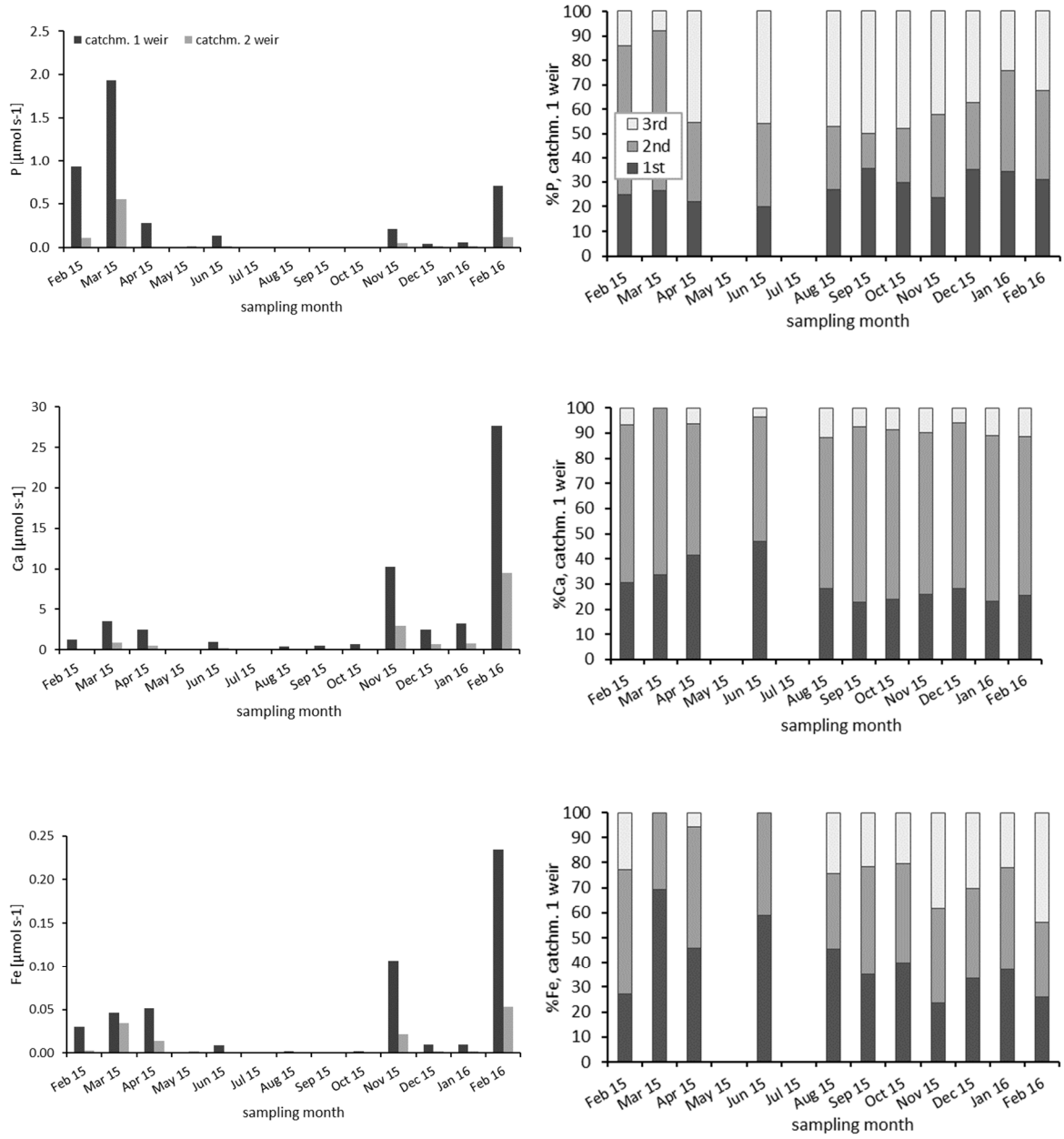

Figure 3: left: All particulate element loads for P, Ca and Fe at both catchments; right: Relative proportions of respective 1st, 2nd and 3rd fraction P, Fe and Ca relative to all colloidal concentrations at catchment 1 weir representative of all sample types. Catchm. = catchment.

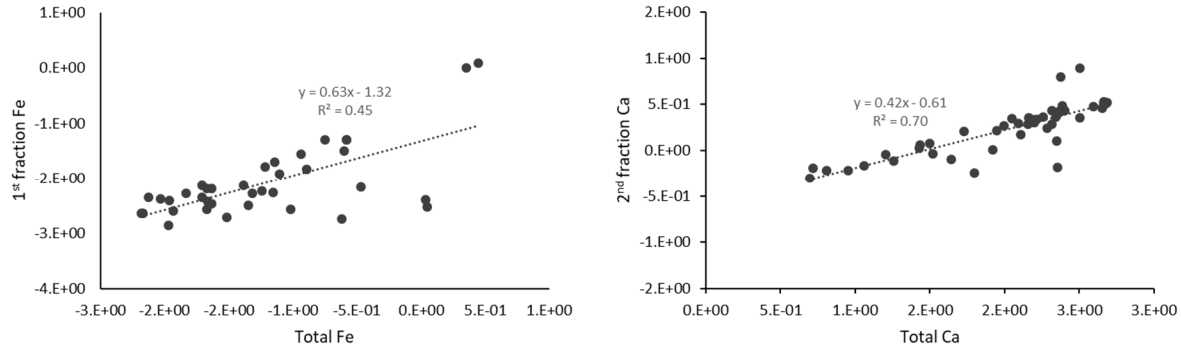

Figure 4: Exemplary relation of colloidal elemental concentration in dependence of total elemental concentrations across all samples taken. Ca and Fe were chosen here to contrast the findings in Gottselig et al. [2017a]. Left: log_{10} transformed data of 1st fraction Fe in dependence of total Fe, right: log_{10} transformed data of 2nd fraction Ca in dependence of total Ca. Unit: µmol/L, n = 65. Compare Table 1, top.

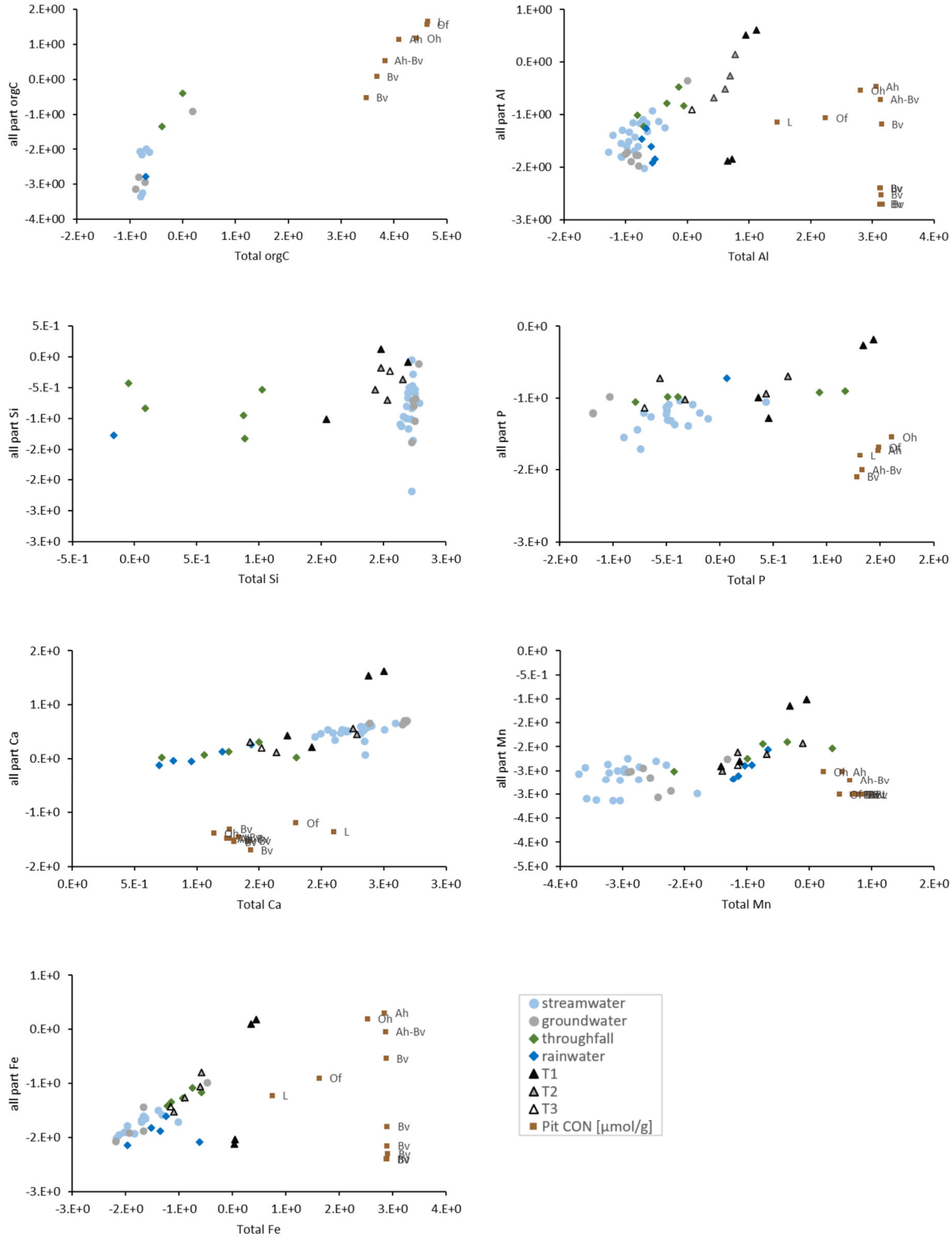

Figure 5: Discrimination of sample types in all colloidal vs. total elemental concentration plots. Concentrations of aqueous samples in µmol L^{-1} were log_{10} transformed prior to visualization. Samples of the soil pit were taken in Nov 13, all colloidal concentration data of the water dispersible colloids (WDC) was taken from Missong et al. (2018a) and total concentrations from Lang et al. (2017), both data sets were transferred to the unit µmol g_{soil}^{-1} for better comparison.